



**HAL**  
open science

# Spectral Directional and Total Hemispherical Emissivity of Virgin and Oxidized 316L Stainless Steel from 1000 to 1650 K

M. Balat-Pichelin, Jean-Louis Sans, E. Beche

► **To cite this version:**

M. Balat-Pichelin, Jean-Louis Sans, E. Beche. Spectral Directional and Total Hemispherical Emissivity of Virgin and Oxidized 316L Stainless Steel from 1000 to 1650 K. *Infrared Physics and Technology*, 2022, 123, pp.104156. 10.1016/j.infrared.2022.104156 . hal-04751022

**HAL Id: hal-04751022**

**<https://cnrs.hal.science/hal-04751022v1>**

Submitted on 13 Nov 2024

**HAL** is a multi-disciplinary open access archive for the deposit and dissemination of scientific research documents, whether they are published or not. The documents may come from teaching and research institutions in France or abroad, or from public or private research centers.

L'archive ouverte pluridisciplinaire **HAL**, est destinée au dépôt et à la diffusion de documents scientifiques de niveau recherche, publiés ou non, émanant des établissements d'enseignement et de recherche français ou étrangers, des laboratoires publics ou privés.



Distributed under a Creative Commons Attribution - NonCommercial 4.0 International License

## **Spectral directional and total hemispherical emissivity of virgin and oxidized 316L stainless steel from 1000 to 1650 K**

M. Balat-Pichelin \*, J.L. Sans, E. Bêche

Laboratoire PROMES-CNRS, UPR 8521, 7 rue du four solaire, 66120 Font-Romeu Odeillo (France)

\*Corresponding author: [Marianne.balat@promes.cnrs.fr](mailto:Marianne.balat@promes.cnrs.fr)

Ph.: +33 468 307 768

### **Abstract**

The 316L stainless steel is used in spacecraft. In order to mitigate debris in the Low-Earth Orbit and to avoid dramatic collisions on Earth after atmospheric re-entry at its end-of-life, the spacecraft mission has to take into account the influence of reentry on the spacecraft survivability. In this way, the emissivity of 316L stainless steel samples: as-received (virgin), pre-oxidized in air plasma and oxidized in situ in air was measured from 1000 K up to 1650 K – as no data can be found in the literature at such high temperatures – and in different atmospheres: high vacuum and for two low total pressures of 300 and 2000 Pa concerning the aerospace domain. Moreover, as it could be interesting for other applications, emissivity measurements at atmospheric pressure were also performed. Experimental results obtained for this material at high temperatures and different pressure conditions together with microstructural characterization using SEM, XRD, Raman spectroscopy and 3D profilometry are presented. As expected, the emissivity of the oxidized 316L samples is much higher than the one measured in high vacuum and there are also some differences between air plasma and standard air conditions – in reduced atmospheres of 300 and 2000 Pa – with respective emissivity increase by a factor 3 and 2.5 in comparison with the virgin material, due to the different levels of oxidation. For the measurements carried out at atmospheric pressure, the increase of the emissivity is also 3 times higher compared to the virgin alloy.

**Keywords:** emissivity; high temperature; 316L stainless steel; oxidation; air plasma

### **1. Introduction**

Materials used for future spacecraft missions must obey to specific rules such as the LOS (Loi relative aux Opérations Spatiales, France), Clean Space Initiative of ESA... in order to be mainly or totally destroyed under the effect of the severe aero-thermodynamic and aero-thermochemical conditions encountered during the atmospheric re-entry. The non-equilibrium

air plasma flow impinging the spacecraft materials enhances oxidation phenomena and also heat flux by species recombination and/or emissivity increase. Oxidation, ablation and melting phenomena can occur on the material leading to an important increase of the temperature and damage of the materials.

To study and to assess the debris survival risks during re-entry, CNES (Centre National d'Etudes Spatiales, France) has developed its own engineering code, DEBRISK [1, 2]. It allows calculating the 3D trajectory of the satellite components, the surface heat flux and the debris disappearance altitudes during the re-entry. However, databases currently available in DEBRISK are limited for oxidation kinetics laws and for the thermal radiative properties (emissivity) of materials at high temperature, parameters needed for the calculation of the final mass reaching the ground. To increase the calculation accuracy of the DEBRISK code, CNES collaborates with PROMES-CNRS laboratory to perform oxidation in atmospheric re-entry conditions and to measure emissivity at high temperature. Oxidation kinetic laws and emissivity data obtained will be implemented in the DEBRISK code. This paper is focused on the evolution of the emissivity of 316L stainless steel versus temperature up to the melting point.

In the literature, few studies are dedicated to the emissivity of the 316L stainless steel especially at high temperature. Isetti and Nannei have investigated the normal total emissivity from 400 K to 1050 K of 316L samples pre-oxidized in air at 1100 K during 3 h and 14 h and the effect of the surface finishing done by mechanical or hand-polishing [3]. The emissivity goes from 0.45 at 400 K up to 0.55 at 1050 K for the samples pre-oxidized during 3 h and respectively 0.60 and 0.75 after 14 h oxidation. Jones and Nisipeanu have measured the spectral (2-10  $\mu\text{m}$ ) directional emissivity of oxidized 316L samples in air at atmospheric pressure, from 773 to 973 K [4]. They conclude that the emissivity decreases when wavelengths increase, for example the normal spectral emissivity for a fully-oxidized sample is going from 0.57 at 2  $\mu\text{m}$  down to 0.18 at 10  $\mu\text{m}$  as the formation of a thin oxide layer (2-3  $\mu\text{m}$ ) composed of  $\text{Cr}_2\text{O}_3$  has an effect relative to the wavelength. For shorter wavelengths (2-6  $\mu\text{m}$ ) of the order of the oxide layer thickness, the emissivity is quite high (0.40-0.50) and for longer wavelengths, this oxide layer is semi-transparent as the behavior of the emissivity is more characteristic of a metal (increase at high angles). Cao et al. have also measured the normal spectral emissivity of 316L samples in air from 773 to 973 K in the wavelength range 2-12  $\mu\text{m}$  [5]. At 773 K, the emissivity is around 0.35 and increases up to 0.50 at 973 K. These low values of emissivity are due to the formation of a thin passive oxide layer made of  $\text{Cr}_2\text{O}_3$  that is semi-transparent and thus the main contribution to the emissivity is due to the metal

and less to the oxide. Shi et al. have only measured the normal emissivity at 1.5  $\mu\text{m}$  in air from 800 to 1100 K [6]. During oxidation, the emissivity increases with heating time, and they obtain after 4 h constant values of 0.67 at 800 K up to 0.81 at 1100 K. Two more recent works of Hunnewell et al. [7] and Al Zubaidi et al. [8] have respectively measured the total hemispherical emissivity of 316L samples and they have shown the effect of roughness and oxidation. Hunnewell et al. have measured the total hemispherical emissivity also in vacuum and they obtain values of 0.26 at 430 K up to 0.36 at 1150 K. Increasing the roughness leads to values of 0.47 for the higher temperature. Then oxidation was performed on samples at 973 K in air during 15 min, and the values goes from 0.37 at 700 K up to 0.60 at 1150 K. Finally, Al Zubaidi et al. measured the total hemispherical emissivity of 316L samples in the range 430-1100 K after long-term oxidation up to 3000 h at 500 K and their results agree with the ones of Hunnewell et al. with values going from 0.25 at 430 K up to 0.34 at 1030 K. They conclude that the oxidation temperature has a strongest effect rather than time on the oxide layer growth and hence the change in emissivity of the material.

Finally, it can be seen that there is no data available at temperatures higher than 1150 K for the austenitic steel 316L. Moreover the oxidation performed on this material was only done in air and never carried out in dissociated gases, in the presence of atomic species such as atomic oxygen. This is why we have measured the spectral directional emissivity and calculated the total hemispherical emissivity for different surface states of 316L samples: virgin ones, measured in high vacuum, some pre-oxidized in air plasma conditions and others in situ oxidized in air in the temperature range 1000-1650 K.

## 2. Experimental emissivity measurement method and device

The direct method used at PROMES-CNRS laboratory is the one that corresponds directly to the definition of emissivity: the directional spectral radiance ( $L'_\lambda$ ) of the material is measured as well as its temperature, the spectral radiance of the blackbody ( $L^0_\lambda$ ) is calculated at the same temperature [9-10]. By definition, the ratio of the radiances gives the spectral directional emissivity:

$$\varepsilon'_\lambda = L'_\lambda / L^0_\lambda$$

The corresponding hemispherical spectral emissivity  $\varepsilon_\lambda^\Omega$  is then calculated by integration of the directional values:

$$\varepsilon_\lambda^\Omega = \int_0^{\pi/2} \varepsilon'_\lambda \sin 2\theta \, d\theta$$

Finally, the total hemispherical emissivity is obtained by integration of the spectral values.

The instrument used for the radiance measurement can be either a radiometer (0.6-40  $\mu\text{m}$ ) or a spectro-radiometer (0.4-14  $\mu\text{m}$ ) that allows measurements at multiple discrete wavelengths, leading to a finer analysis of the behavior of materials, as for example during oxidation of alloys at high temperature.

The experimental set-up MEDIASE (Moyen d'Essai et de Diagnostic en Ambiance Spatiale Extreme) shown in Figure 1 is placed at the focus of the 1 MW Odeillo solar furnace to reach very high temperature in a few seconds. The set-up consists of a stainless steel vessel with a capacity of  $6 \cdot 10^{-2} \text{ m}^3$ , equipped with a turbo-molecular pumping system allowing working in high vacuum conditions (up to  $10^{-5} \text{ Pa}$ ). A hemispherical window (35 cm diameter) in silica-glass allows the heating of the sample (40 mm diameter, 2 mm thickness) by concentrated solar radiation using the gradual opening of the doors of the solar furnace. The environment is controlled in the set-up: high vacuum – or higher controlled pressure – under chosen atmosphere (air or other gas). The front face of the sample is exposed to the concentrated solar radiation and measurements are made on the rear side of the sample, away from incident solar radiation, in an environment at room temperature. It should be noticed that this causes a temperature gradient in the sample: the insulated face must be brought to a temperature significantly higher than that of the measured face, the thermal gradient depending essentially on the thermal conductivity and the thickness of the sample. The true temperature of the sample is measured on the back face using a two-color pyro-reflectometer developed in our laboratory [11]. This instrument is calibrated on a blackbody whose temperature can reach 1900 K measured with a standard pyrometer. The temperature of the samples is given with an average relative uncertainty of 2% between 1100 and 1900 K. The radiance measurements are carried out using either a radiometer (Heimann KT4, wavelength range 0.6-40  $\mu\text{m}$ ) or a spectro-radiometer (CI systems, SR-5000N) equipped with an optic allowing, at the measurement distance used, to observe an area of 9 mm diameter at normal incidence in the center of the sample. For the spectro-radiometer, the spectral domain studied (0.4-14  $\mu\text{m}$ ) does not make it possible to work with a single detector thus two systems are present: a spectro-photometer working from 0.46 to 1  $\mu\text{m}$  and a spectro-radiometer operating from 1.3 to 14  $\mu\text{m}$ . We have a blind zone between 1 and 1.3  $\mu\text{m}$ . It produces signals spaced about 36 nm in the range 1.3 to 14  $\mu\text{m}$  and 0.4 nm in the range 0.46-1  $\mu\text{m}$ , respectively 354 and 990 wavelengths which is enough to calculate the radiances for the chosen spectral bands. The measurements are carried out through an original 3-mirrors angular positioner (goniometer) developed at PROMES-CNRS - the sample, the spectro-radiometer and the optical window

remaining fixed - at incidence angles from  $0^\circ$  to  $80^\circ$  by  $10^\circ$  step plus  $45^\circ$  and  $75^\circ$  for samples of 40 mm diameter. The nature of the optical window is adapted to the wavelength range studied and in that case, it is made of thallium iodo-bromide (KRS5). The spectro-radiometer - goniometer - optical window assembly is calibrated before the series of tests, in front of a blackbody whose temperature is measured with a standard pyrometer. The uncertainties of the emissivities change as a function of the temperature and of their spectral and/or directional quantities. For temperatures between 1100 and 1600 K, we typically obtain directional spectral relative uncertainties of 10% at  $2\ \mu\text{m}$ , 4% at  $10\ \mu\text{m}$ , and 5% for the total hemispherical emissivity.

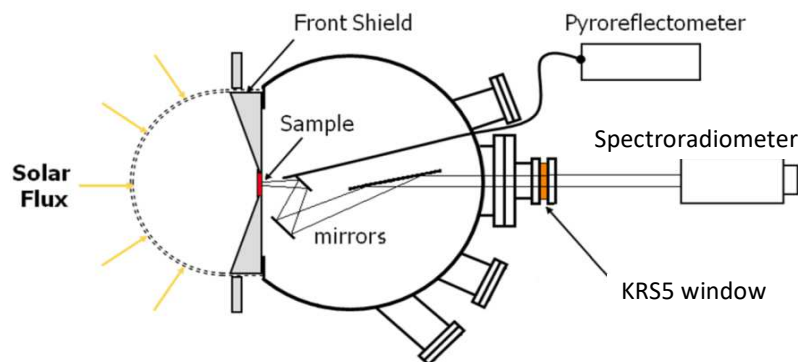
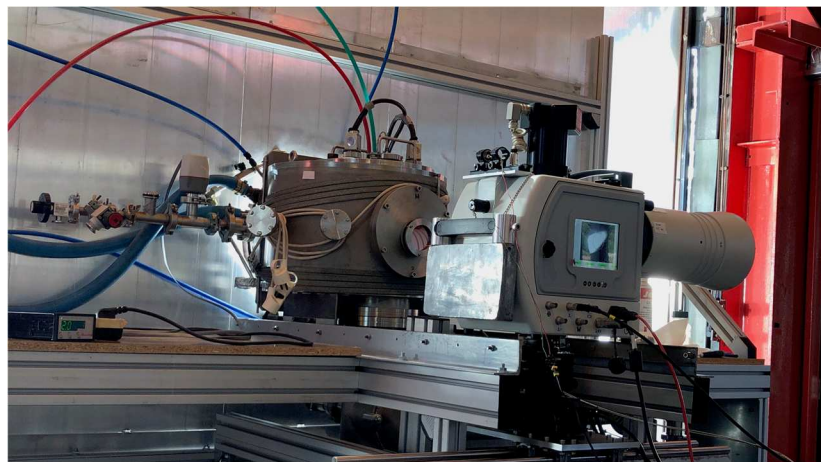


**Figure 1:** Photo and scheme of the MEDIASE set-up with the spectro-radiometer at the focus of the 1000 kW solar furnace

### 3. Material and characterization methods

The 316L samples were delivered by Goodfellow, France. They were disks of 25 and 40 mm diameter and 2 mm thickness. Some of them were sand-blasted to see the effect of the surface roughness on emissivity. The 25 mm diameter samples were pre-oxidized in air plasma

conditions to simulate the surface state that can be encountered during an atmospheric re-entry of space debris. The composition of the 316L samples is reported in Table 1 and the initial surface roughness of the samples is given in Table 2.

**Table 1:** Elementary composition of the 316L stainless steel

SS 316 L Goodfellow	Fe	Cr	Ni	Mn	Mo	Si	C	S	P	N
	balance	17.000	12.000	2.000	2.500	0.750	0.030	0.030	0.045	0.010

**Table 2:** Surface roughness parameters  $S_q$  and  $S_z$  of the as-received and sand-blasted samples

Reference sample	$S_q$ ( $\mu\text{m}$ )	$S_z$ ( $\mu\text{m}$ )
316L as-received	0.64	15.23
316L sand-blasted (2 different samples)	1.16 - 2.03	15.82 - 28.33

The samples were characterized before and after emissivity measurement by SEM and EDS (Hitachi SEM-FEG-S-4500), XRD (PANalytical X'Pert PRO MPD ( $\theta$ - $\theta$ )), Raman spectroscopy (HORIBA LabRAM HR evolution) and 3D profilometry (Leica DCM 3D).

#### 4. Experimental results and discussion

The sample placed in a cooled sample-holder and maintained by three needles to minimize the heat transfer is inserted in the experimental device MEDIASE and the vacuum is done using a primary pump and/or a turbo-molecular pump for secondary vacuum. Then, the pressure is fixed according to the chosen experiment:  $10^{-3}$ - $10^{-4}$ , 300 or 2000 Pa with flowing air, or atmospheric pressure (static air). The sample is heated by the gradual opening of the doors of the solar furnace up to the desired temperature level. This could be done in a few seconds. When the temperature is stable, the directional measurement of the radiance (mean value of 3 scans) of the sample is done and also of the temperature. Then, the temperature is increased up to the next level of around 100 K higher. After the highest temperature level reached, some measurements are carried out at lower temperatures to prove that the oxide layer formed at high temperature is stable, and that the emissivity stays high due to the presence of this oxide layer.

##### 4.1. Emissivity in high vacuum

The emissivity of the virgin as-received samples was measured in high vacuum ( $10^{-3}$ - $10^{-4}$  Pa). Figure 2 presents an example of the evolution of the spectral emissivity for a 316L sample

measured in high vacuum at 1283 K. For all the directions, the spectral emissivity is decreasing when the wavelength increases in agreement with the electromagnetic theory for metals, going from around 0.30-0.40 at 1.5  $\mu\text{m}$  down to 0.15-0.20 from 6 to 14  $\mu\text{m}$ , and also in agreement with the literature data. Figure 3 presents the results obtained for the total hemispherical emissivity for the 316L samples as-received and sand-blasted (s), the data presented are only those obtained when increasing the temperature. The emissivity is decreasing linearly for the as-received samples from 1100 K up to 1400 K going from around 0.35 down to 0.25 and this could be explained by the decreasing surface roughness  $S_q$  of the samples going from the reference of  $0.64 \pm 0.01$  down to  $0.56 \pm 0.02$  (mean value for samples 1G, 7G and 9G) due to the smoothing of the surface as revealed by the SEM images (Figure 4). For the sand-blasted surfaces, the emissivity is a little bit higher but above 1300 K, the values are of the same order as for the as-received samples due also to the smoothing of the surface. The surface roughness  $S_q$  is going from  $2.03 \pm 0.02 \mu\text{m}$  down to  $1.85 \pm 0.03 \mu\text{m}$  and the  $S_z$  is also decreasing from  $28.33 \pm 3.00 \mu\text{m}$  down to  $23.21 \pm 2.00 \mu\text{m}$ .

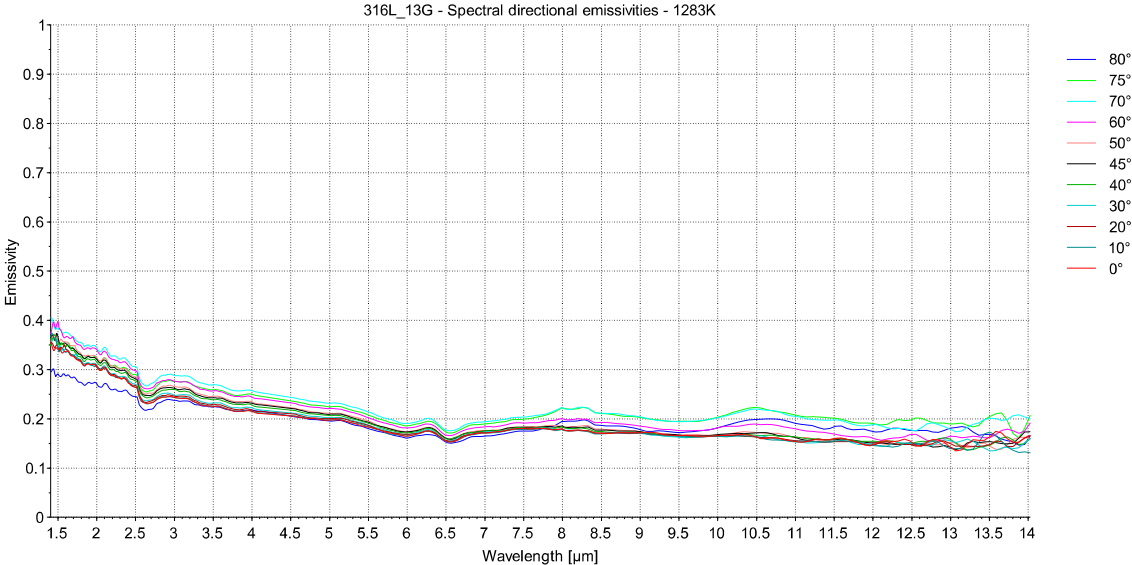


**Figure 2.** Evolution of the spectral directional emissivity for a 316L sample at 1283 K in high vacuum conditions



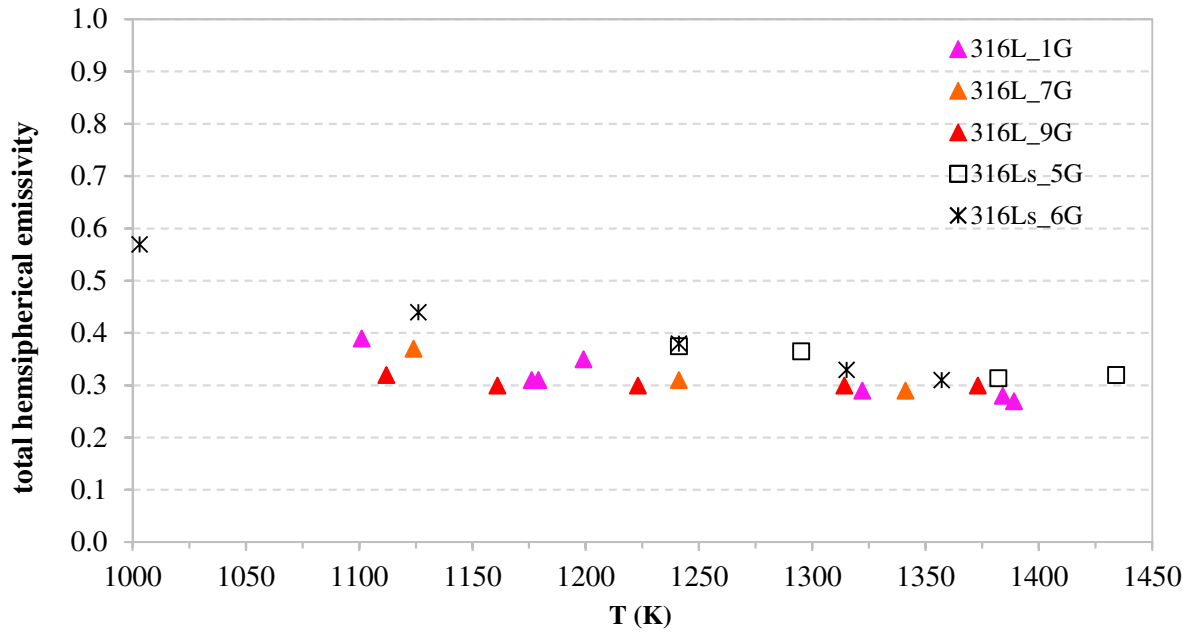


**Figure 3.** Evolution of the total hemispherical emissivity for the 316L samples (s is for sand-blasted samples) versus temperature

The total hemispherical emissivity obtained on the as-received samples is in good agreement with the one measured by Hunnewell et al. at 1150 K with respectively values of around 0.35 for us and 0.36 for [7].

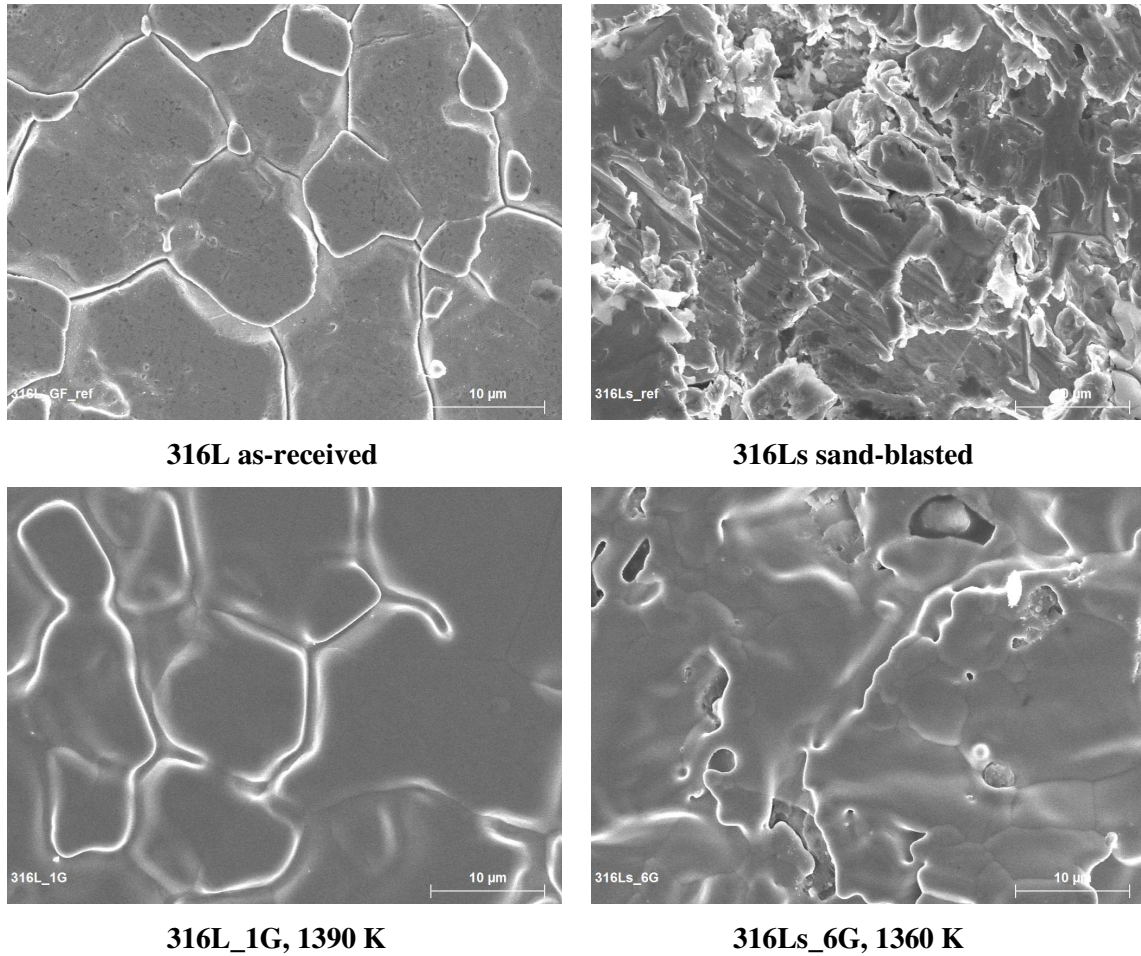


**Figure 4.** SEM images of the samples: reference, before emissivity measurement and after with the maximum temperature reached (magnification x 2500)

#### 4.2. Emissivity measured on pre-oxidized samples

To be compliant with atmospheric re-entry conditions, some samples were pre-oxidized in air plasma as already done for Inconel 718 [12], Invar [13] and TA6V [14, 15] samples. Then, the normal spectral emissivity was measured on each sample in the same conditions of total air pressure. The pre-oxidized samples are 25 mm diameter so only the normal spectral or total radiance is measured during experiment due to the size of the sample. Figure 5 reports the evolution of the total normal emissivity versus temperature for the pre-oxidized samples – during 300 s on the temperature plateau – at 300 and 2000 Pa total air pressure, measured with the radiometer (0.6-40 μm) or with the spectro-radiometer (1.4-14 μm, referred as ‘\_sp’). The emissivity is thus quite high, going from around 0.80 at 1100 K up to nearly 0.95 at 1650 K, as an oxide layer was already formed during the oxidation in air plasma conditions and it can be seen that a linear fit can be derived leading to:

$$\varepsilon = 2.1 \times 10^{-4} T + 0.5807 \quad R^2 = 0.62$$

The influence of the total pressure – 300 or 2000 Pa – has no effect on the evolution of the emissivity as the oxide layers are of same composition, the main influent factor being the temperature.

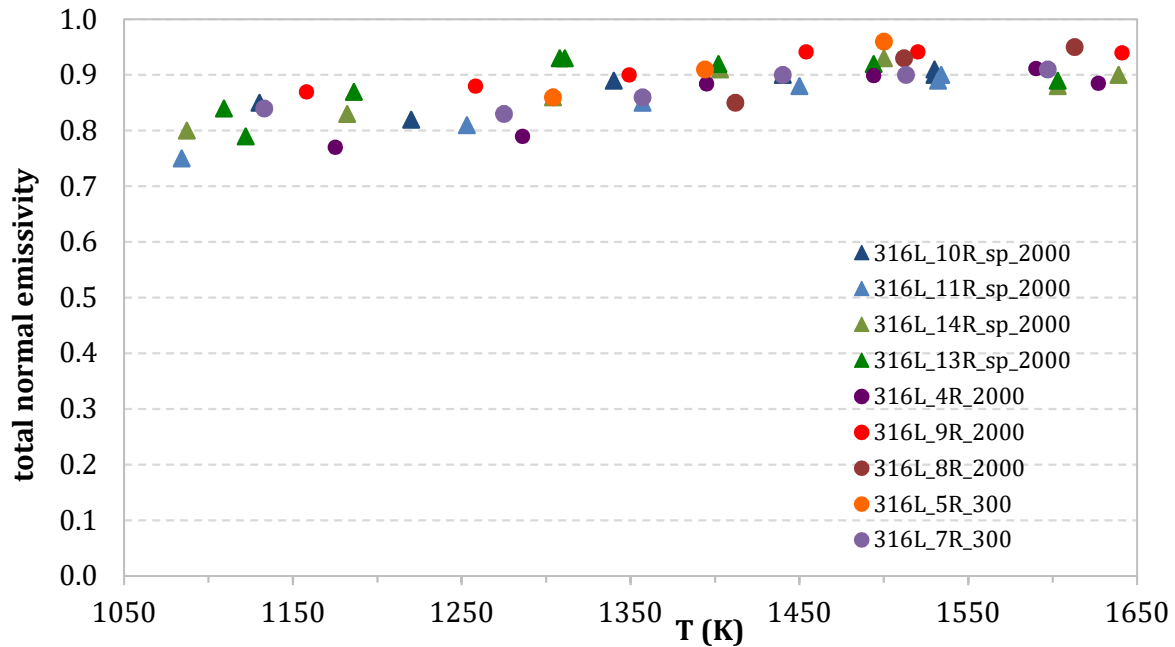
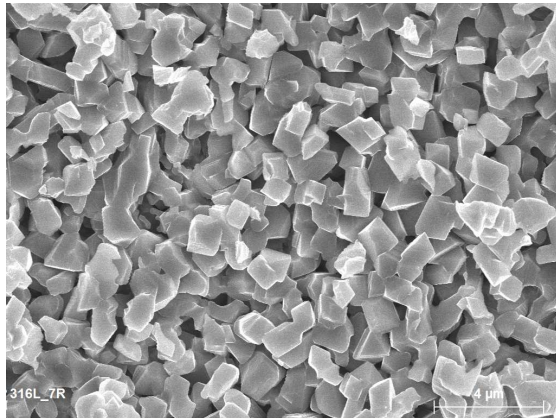


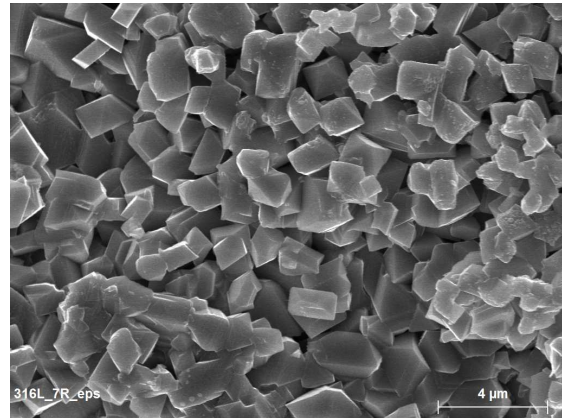
**Figure 5.** Evolution of the total normal emissivity versus temperature for the pre-oxidized samples under air plasma at 300 and 2000 Pa. Measurements carried out with the spectro-radiometer are marked by a triangle and ‘\_sp’ and those made using the radiometer are marked by a dot

The high temperature pre-oxidation was done up to 1550 K for samples 5R, 10R\_sp and 11R\_sp and up to 1680 K for all the other samples. The measurement of emissivity after the high temperature oxidation of the samples has not modified the surface morphology as confirmed by the SEM images shown in Figure 6. Moreover, the surface roughness of the samples was maintained with, for example, respective Sq values for before/after emissivity measurement of 1.97/2.24  $\mu\text{m}$  for the sample 316L\_8R pre-oxidized at 2000 Pa and 3.02/3.69  $\mu\text{m}$  for the sample 316L\_7R pre-oxidized at 300 Pa, both up to 1650 K. XRD patterns presented in Figure 7 have also proved that no structural modification has occurred after the emissivity measurement. Into the depth of the analysis zone by XRD – around 10  $\mu\text{m}$  - the oxide layer is mainly composed of hematite  $\text{Fe}_2\text{O}_3$  (ICDD 84-0309) and magnetite  $\text{Fe}_3\text{O}_4$  (ICDD 80-6406), regardless the pressure levels. However, Energy dispersive X-ray Spectroscopy (EDS) analyses were carried out on the 316L\_11R sample oxidized in air plasma around 1550 K at 2000 Pa, and more precisely on two different zones: on an oxide

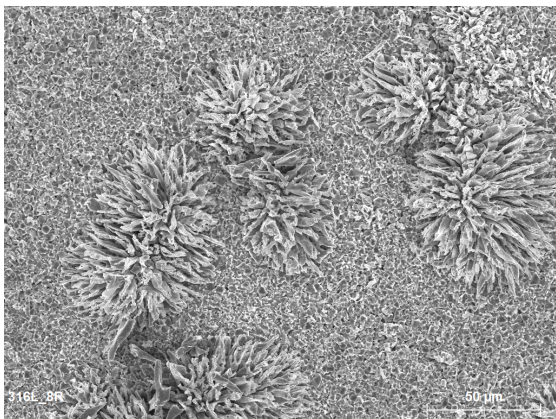
'flower' as well as on the bottom next to the latter (Fig. 6). It can be noticed that EDS analyses concern only the first micron layer of the oxide, on the contrary of XRD analyses. The 'flower' is mainly composed of iron and oxygen with a very small amount of chromium, characteristics of hematite. As for the bottom next to the 'flower', it is mainly composed of chromium and iron, characteristics of the oxides  $\text{Cr}_2\text{O}_3$  and  $\text{Fe}_2\text{O}_3$  or of a mixed oxide  $\text{FeCr}_2\text{O}_4$  (Fig. 8).



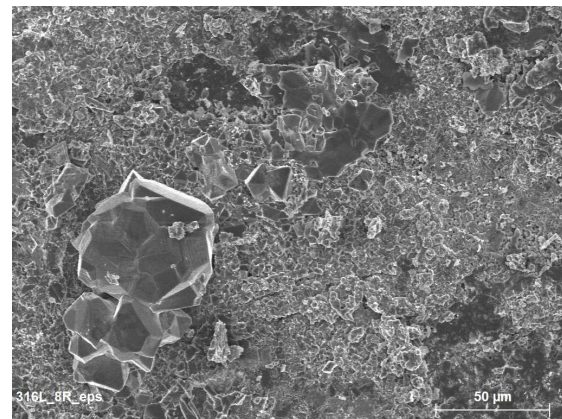
**316L\_7R\_300 Pa before emissivity**



**316L\_7R\_300 Pa after emissivity**



**316L\_8R\_2000 Pa before emissivity**



**316L\_8R\_2000 Pa after emissivity**

**Figure 6.** SEM images of the pre-oxidized 316L samples before and after emissivity measurement at high temperature (magnification x 6000 and x 500)

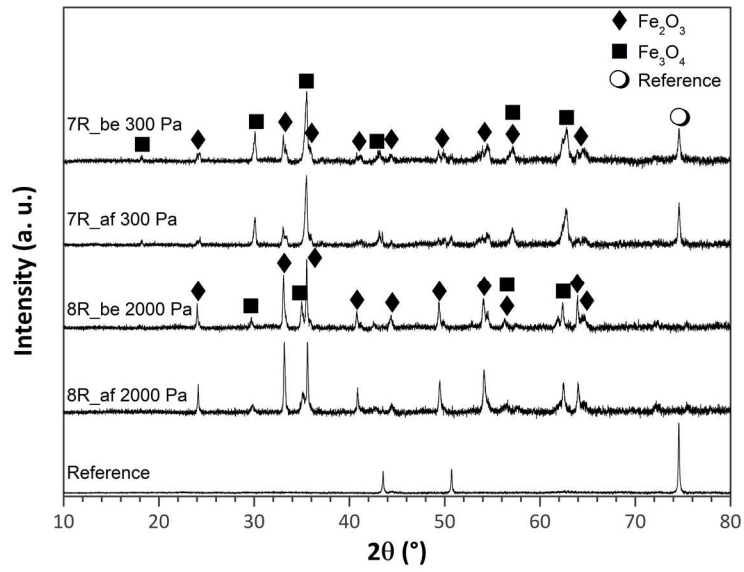


**Figure 7.** XRD patterns of two 316L pre-oxidized samples (7R and 8R) in air plasma conditions before (\_be) and after (\_af) emissivity measurement at two different pressures (300 and 2000 Pa)

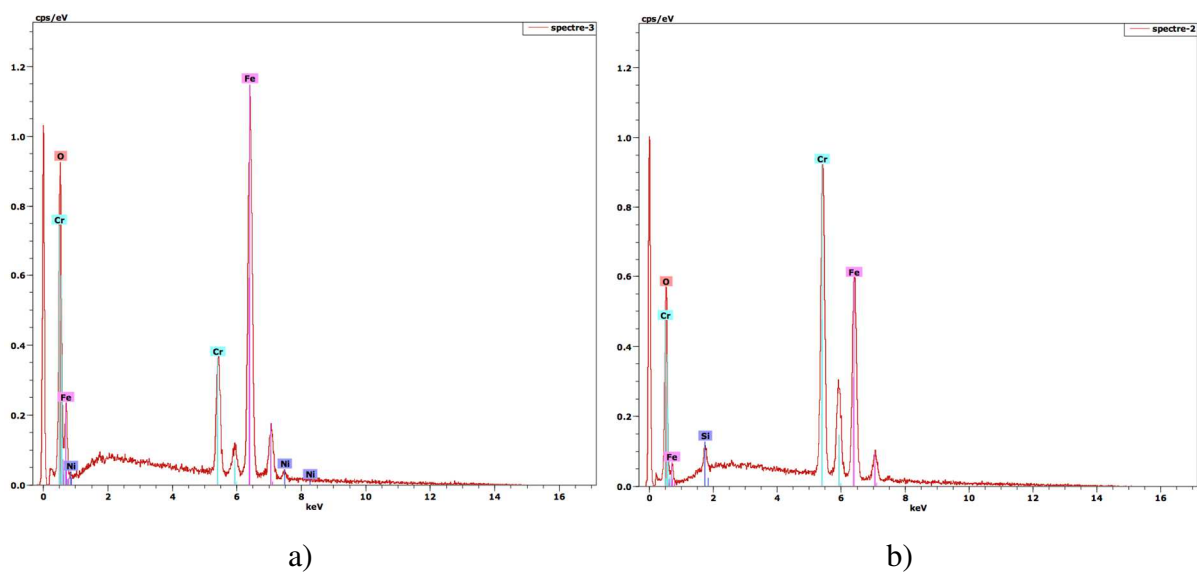
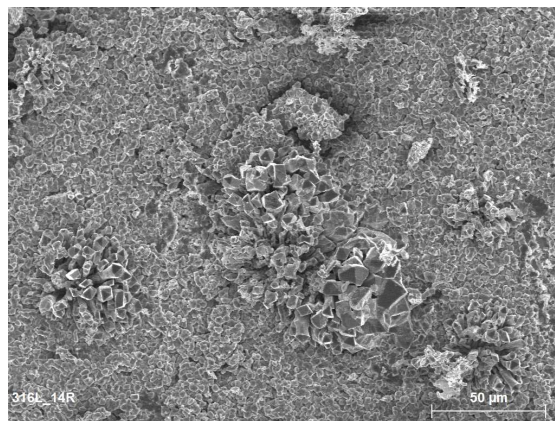


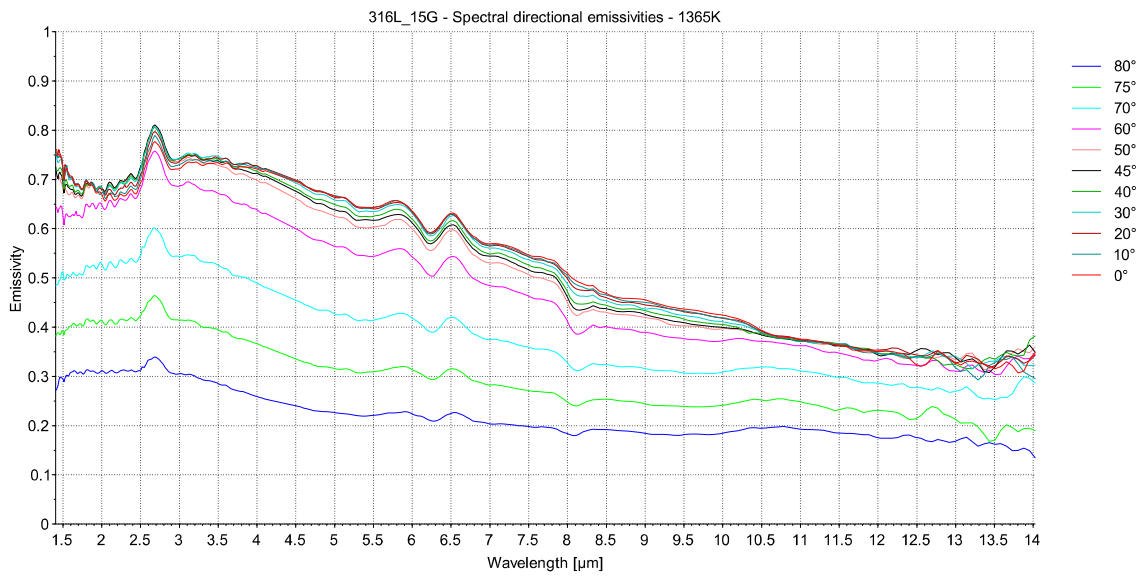
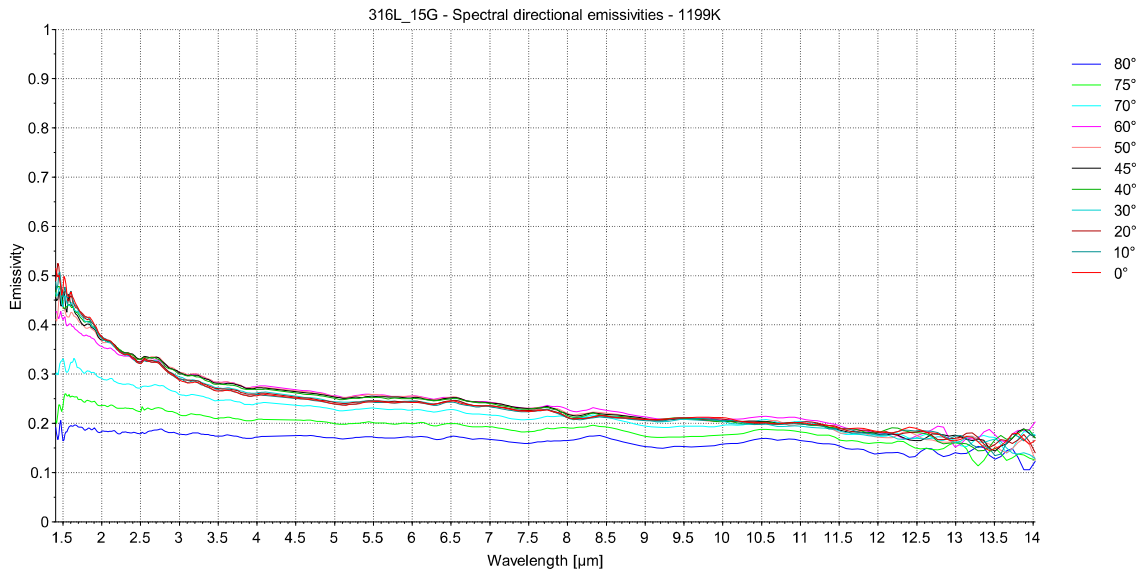
**Figure 8.** SEM image (magnification  $\times 500$ ) and EDS spectra obtained on the 316L\_14R sample pre-oxidized at 1680 K, 2000 Pa taken on a) an oxide 'flower' and b) the other part (bottom)

Finally, the total normal emissivity of oxides formed in air plasma is three times that of the un-oxidized 316L (0.30). Thus, the influence of air plasma oxidation on emissivity must be taken into account in atmospheric re-entry codes for the calculation of the heat flux of space objects made of 316L steel.

### **4.3. Emissivity for samples oxidized in situ**

Other emissivity measurements were performed on 316L samples oxidized in situ in standard air at 300, 2000 Pa and at atmospheric pressure to observe a possible difference in emissivity with the air plasma conditions. An example of the evolution of the spectral emissivity with the oxidation is shown in Figure 9 for several temperatures: 1200, 1365, 1480 and 1920 K. In this figure, it could be mentioned that the contribution of the absorption bands for H<sub>2</sub>O (around 2.7 and 5.2-6.8  $\mu\text{m}$ ) and CO<sub>2</sub> (around 2.7 and 4.2  $\mu\text{m}$ ) are visible and not linked to a material characteristics. Only the CO<sub>2</sub> band in between 4 and 4.5  $\mu\text{m}$  was suppressed in these figures. These bands are more or less visible due to the different environmental conditions during calibration and measurement. For example, for the 316L\_15G sample, during calibration the temperature and relative moisture were respectively of 24°C and 17%, and during the emissivity measurement, they were equal to 14°C and 42%. It appears clearly that the emissivity is increasing in the longer wavelength range when oxidation occurs for the higher temperature levels. The evolution of the total hemispherical emissivity as a function of the temperature for the 316L samples oxidized in situ in standard air for the 3 total pressures in the temperature range 1000-1630 K is reported in Figure 10 where are plotted the results for the as-received samples and the sand-blasted (s) ones, and the SEM images are presented in Figure 11 showing a quite similar morphology. For the as-received samples, the total hemispherical emissivity increases from 0.25 to 0.70 in the 1100-1500 K range due to the oxide formation then stabilizes around 0.75 up to the highest temperature levels. An increase of a factor 2.5 was noted for the emissivity of the samples oxidized in situ under standard air compared to the virgin sample (0.30). For the sand-blasted ones, the total hemispherical emissivity is obviously higher due to the increase roughness of the samples compared to the as-received ones and it is more stable for the lower temperatures, with values of 0.50 around 1000 K up to 0.70 at 1450 K. Then it increases again to reach 0.90 around 1500 K that is stable up to the highest temperature levels. An increase of a factor 3 can be noted for the samples oxidized in situ under standard air at atmospheric pressure compared to the virgin sample (0.30). The emissivity increase for the oxides compared to that of the virgin alloy is therefore more significant in air plasma than in standard air, thus showing the importance of

carrying out emissivity measurements on pre-oxidized samples under air plasma to be used in re-entry codes.



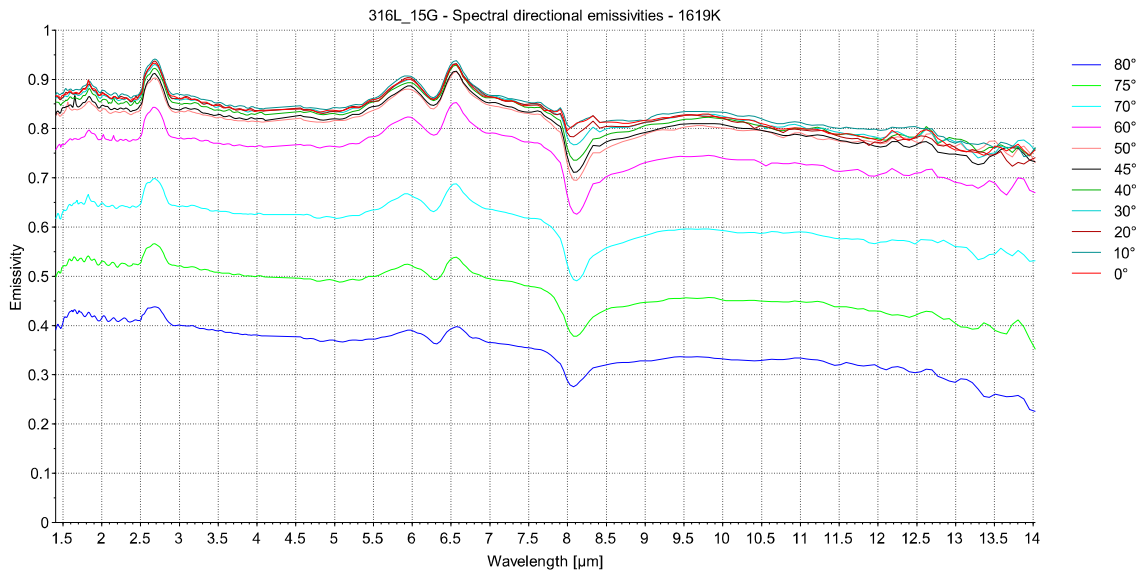
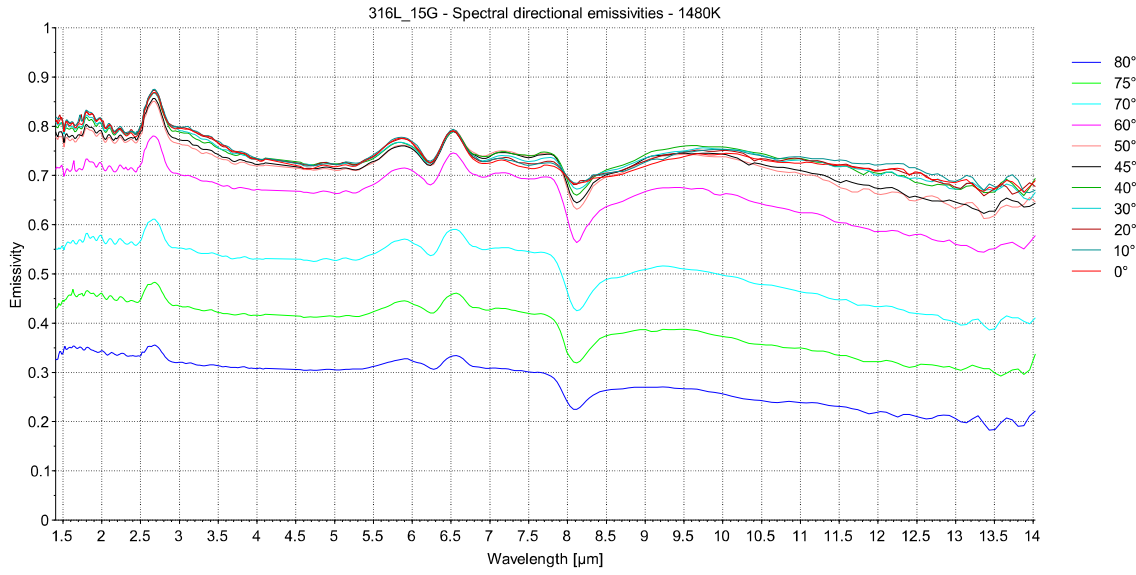


**Figure 9.** Evolution of the spectral directional emissivity for a sample (316L\_15G) oxidized in situ in air at 2000 Pa for different temperatures



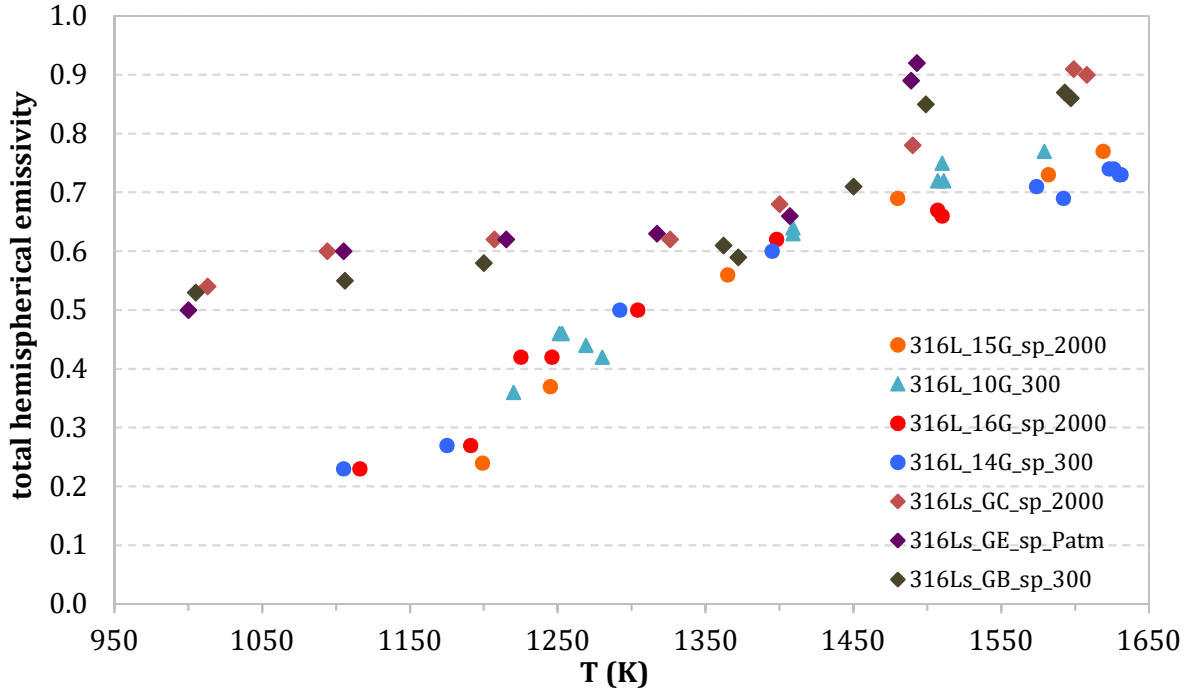


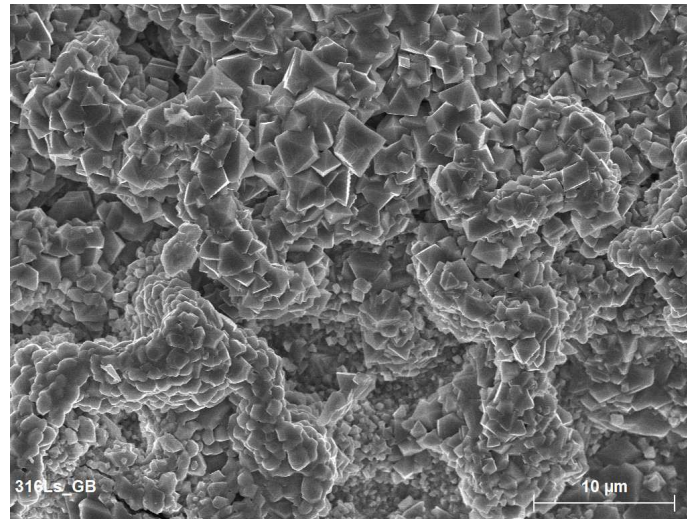
**Figure 10.** Evolution of the total hemispherical emissivity versus temperature for the 316L samples oxidized in situ in air at 300, 2000 Pa and atmospheric pressure (Patm)

**Table 3:** Surface roughness parameters  $S_q$  and  $S_z$  of the in situ oxidized samples

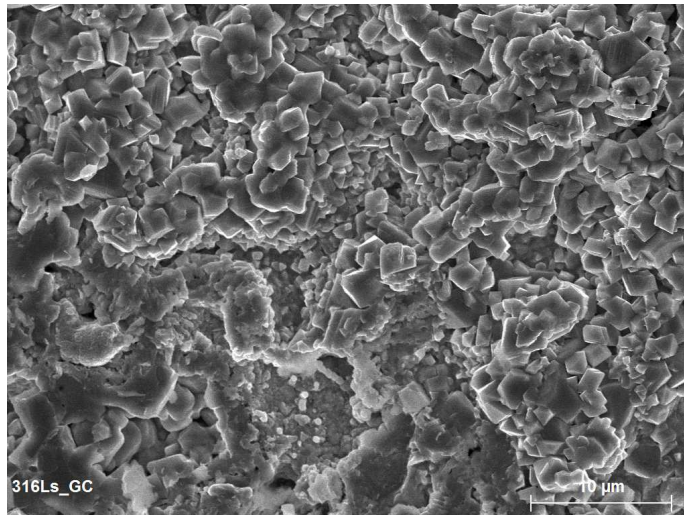
In situ oxidized sample	$S_q$ ( $\mu\text{m}$ )	$S_z$ ( $\mu\text{m}$ )
316L_300 Pa	1.68	19.50
316L_2000 Pa	2.08	22.03
316Ls_2000 Pa	2.48	42.60
316Ls_Patm	4.53	42.53

Table 3 reports the surface roughness parameters of the as-received and sand-blasted samples after emissivity measurement. For the as-received samples (316L\_300 Pa and 316L\_2000 Pa), the surface roughness parameters  $S_q$  and  $S_z$  are higher than for the reference samples (Table 2) due to the presence of the oxide layer but they are close whatever the pressure (300 and 2000 Pa). For the sand-blasted ones, the  $S_q$  is a little bit higher particularly for the measurement carried out at atmospheric pressure and the  $S_z$  is nearly twice its initial value (see Table 2). The surface roughness of the sample 316Ls\_300 is not given as it can be seen in Figure 11 that the surface is very rough with big clusters of grains growing in the Z direction leading to very huge values of  $S_z$  with great discrepancies observed for several measurements. Nevertheless, even if the surface roughness values measured on the oxide

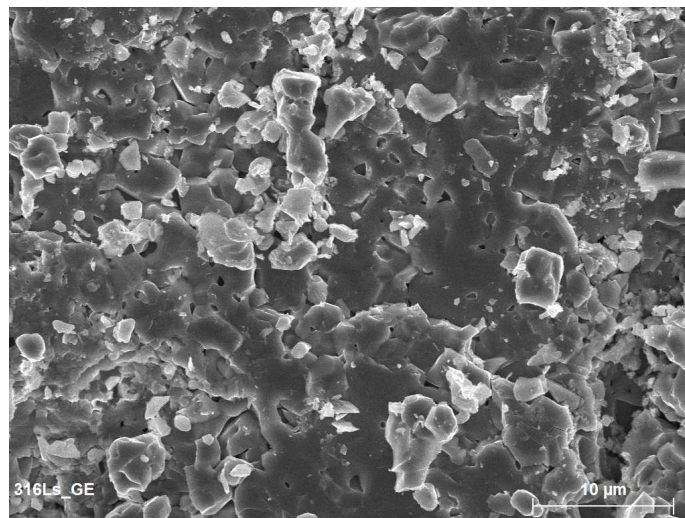
layers are different according to the surface states (as-received and sand-blasted), the evolution of the emissivity is not sensitive to the total air pressure.



*300 Pa*



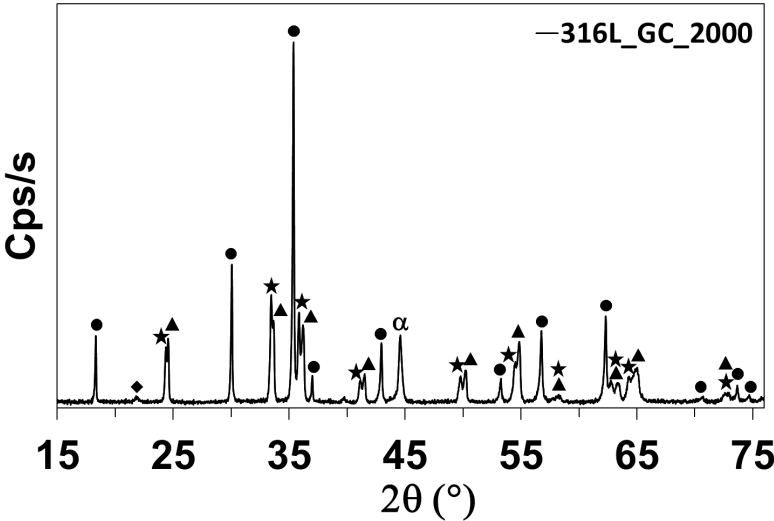
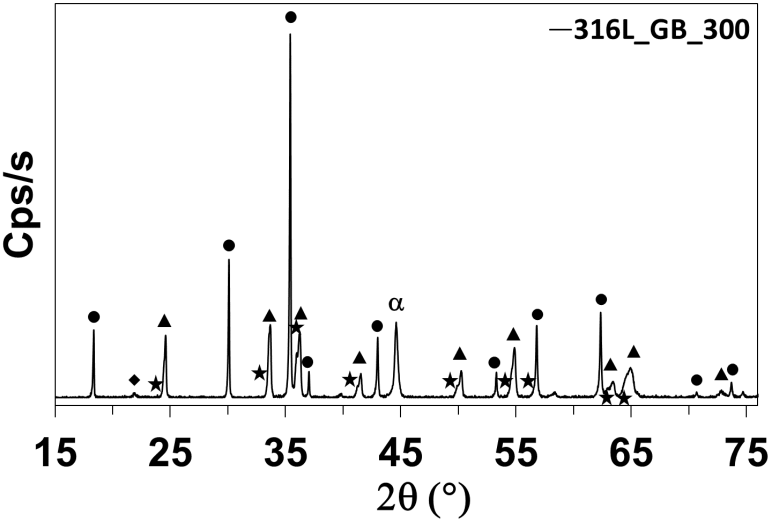
*2000 Pa*



*Patm*

**Figure 11.** SEM images of the 316Ls sand-blasted samples after emissivity measurement at high temperature (magnification x 2500)

XRD analyses and Raman spectroscopy were carried out to characterize the chemical composition of the surfaces of the samples after in situ oxidation. Figure 12 presents the XRD patterns of the samples treated at 300, 2000 Pa and at atmospheric pressure those emissivity data are reported in Figure 10.



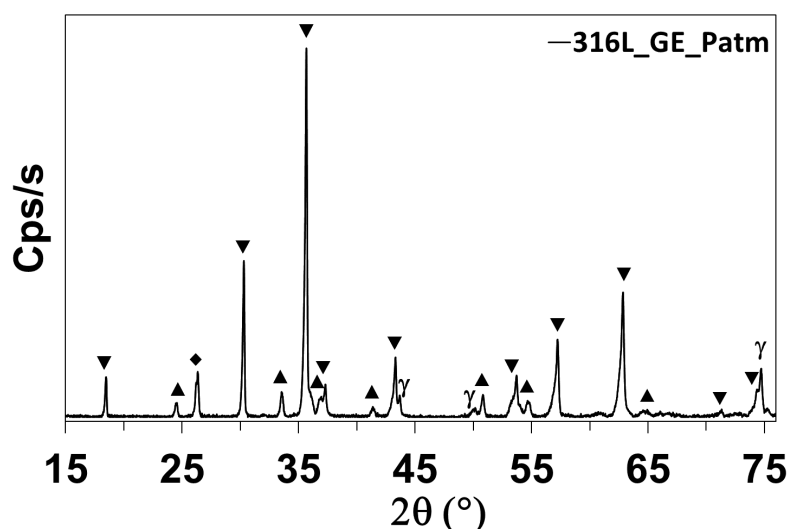


**Figure 12.** XRD patterns of the 316L samples oxidized in situ, obtained after emissivity measurement. The symbols correspond to the following species:  $\gamma$ 316L substrate,  $\blacktriangle$ Cr<sub>2</sub>O<sub>3</sub>,  $\star$  Fe<sub>2</sub>O<sub>3</sub>,  $\blacktriangledown$  NiFe<sub>2</sub>O<sub>4</sub>,  $\bullet$  Fe<sub>3</sub>O<sub>4</sub> and  $\blacklozenge$  SiO<sub>2</sub>.

From these XRD patterns, it appears that for the lowest pressure (300 Pa), the main oxide compounds are magnetite Fe<sub>3</sub>O<sub>4</sub>, Cr<sub>2</sub>O<sub>3</sub> (ICDD 73-4336) and less hematite Fe<sub>2</sub>O<sub>3</sub>. Increasing the pressure to 2000 Pa leads to the same species with an increase of hematite Fe<sub>2</sub>O<sub>3</sub>. At atmospheric pressure, the main compound is the spinel NiFe<sub>2</sub>O<sub>4</sub> (ICDD 86-2267) and less Cr<sub>2</sub>O<sub>3</sub>. So increasing the pressure, the main oxide formed on the 316L goes from magnetite Fe<sub>3</sub>O<sub>4</sub> to the spinel phase NiFe<sub>2</sub>O<sub>4</sub>.

Raman spectroscopy was performed at room temperature on the samples oxidized in situ such as for the XRD analysis. Raman spectra were recorded in the wavenumber range 150-1200 cm<sup>-1</sup>. The excited source is a 532 nm laser beam and the laser power was reduced to about 8 mW (filter 25%) to avoid laser-induced effects. They were collected at the focal point of the objective lens (x50 or x100) with a spectral resolution close to 1 cm<sup>-1</sup>/pixel. The 1800 grating and the confocal pinhole value of 50 or 100 μm were selected. The acquisition time and the number of acquisition by spectra were respectively fixed at 20 s and 5. For the sample oxidized at 300 Pa (GB, Figure 12), the surface is composed of the spinel Fe<sub>x</sub>Cr<sub>2-x</sub>O<sub>4</sub> and Cr<sub>2</sub>O<sub>3</sub>, and less hematite Fe<sub>2</sub>O<sub>3</sub> (Figure 13). In Figure 13 a), the Raman peak at 675 cm<sup>-1</sup> is assigned to the A<sub>1g</sub> symmetric stretching vibration mode of the Fe<sup>III</sup>, Cr<sup>III</sup>-O bonds of the (Fe<sup>3+</sup>, Cr<sup>3+</sup>)-O<sub>6</sub> octahedra (Fe<sub>x</sub>Cr<sub>2-x</sub>O<sub>4</sub> chromite spinel) [16-18]. The shoulder in the 620-660 cm<sup>-1</sup> region is mainly assigned to the A<sub>1g</sub> vibration mode. This mode is strongly affected by the cation substitution in the octahedral site leading to a cation disorder in the octahedral sites. This shoulder could be related to the cation-anion bond lengths and polyhedral distortion

occurring in the non-stoichiometric chromite. The wide peak in the 480-560  $\text{cm}^{-1}$  region revealed two summits located at 525 and 555  $\text{cm}^{-1}$ :

- the Raman peak at about 525  $\text{cm}^{-1}$  is attributed to  $F_{2g}(2)$  lattice modes of Fe and O atoms in Fe-O bonds ( $\text{Fe}_x\text{Cr}_{2-x}\text{O}_4$  chromite spinel) [18].

- the Raman peak detected at about 555  $\text{cm}^{-1}$  is assigned to  $A_{1g}$  vibration mode of the  $\text{Cr}^{\text{III}}\text{-O}$  bonds ( $\text{Cr}^{3+}$  ions in octahedral coordination) of a  $\text{Cr}_2\text{O}_3$  compound [19, 20],

In Figure 13 b), the Raman spectrum corresponds to the measurement done on a shiny grain and the sample surface. It mainly exhibits several bands attributed to  $\text{Cr}_2\text{O}_3$ , a  $\text{Fe}_x\text{Cr}_{2-x}\text{O}_4$  chromite type spinel or a non-stoichiometric  $\text{Fe}_x\text{Fe}_{2-x}\text{O}_4$  spinel and  $\text{Fe}_2\text{O}_3$ . For the sample oxidized at 2000 Pa (GC, Figure 12), the same species were detected as shown in Figure 14, and for the sample oxidized at atmospheric pressure (GE, Figure 12), the two spinels  $\text{Fe}_x\text{Cr}_{2-x}\text{O}_4$  and  $\text{Ni}_x\text{Fe}_{2-x}\text{O}_4$  were detected (Figure 15). The Raman spectrum mainly exhibits several bands attributed to a  $\text{Fe}_x\text{Cr}_{2-x}\text{O}_4$  chromite spinel and a  $\text{Ni}_x\text{Fe}_{2-x}\text{O}_4$  trevorite spinel [21, 22]. The shoulders located around 645 and 703  $\text{cm}^{-1}$  are assigned to the  $A_{1g}$  symmetric stretching vibration mode of the  $\text{Fe}^{\text{III}},\text{Cr}^{\text{III}}\text{-O}$  bonds of the  $(\text{Fe}^{3+},\text{Cr}^{3+})\text{-O}_6$  octahedra in disordered  $\text{Ni},\text{Fe}_x\text{Cr}_{2-x}\text{O}_4$  spinel. These results are in quite good agreement with the XRD analysis even if the two analyzed depth zones are different: around 10  $\mu\text{m}$  for XRD and only 1  $\mu\text{m}$  for Raman.

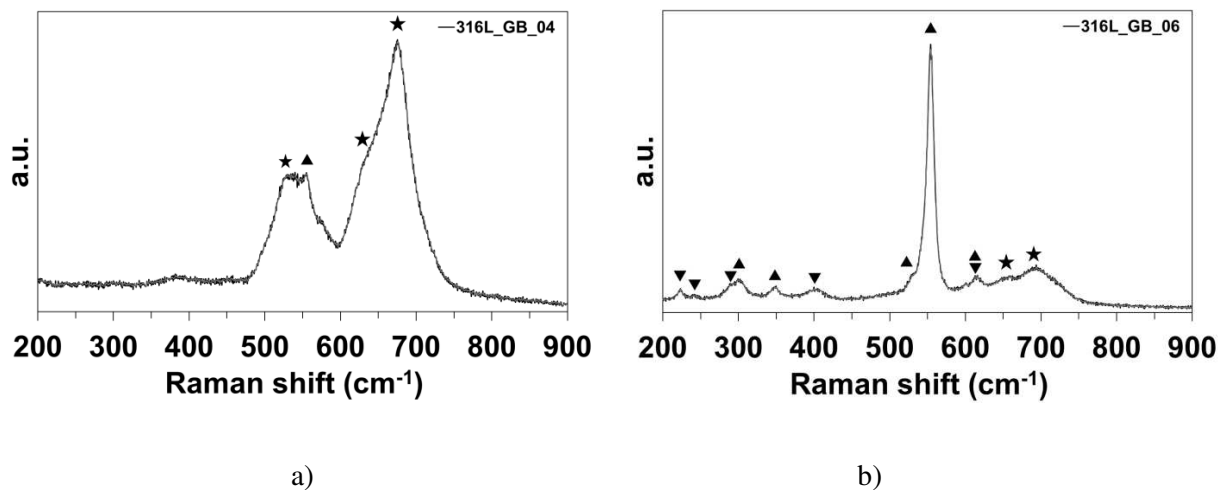


**Figure 13.** Raman spectra for the 316Ls sample oxidized in situ at 300 Pa, after emissivity measurement at different locations on the surface: \_04 characteristics of the main surface, and \_06 on a shiny grain ( $\blacktriangle \text{Cr}_2\text{O}_3$ ;  $\star$  Spinel;  $\blacktriangledown \text{Fe}_2\text{O}_3$ )

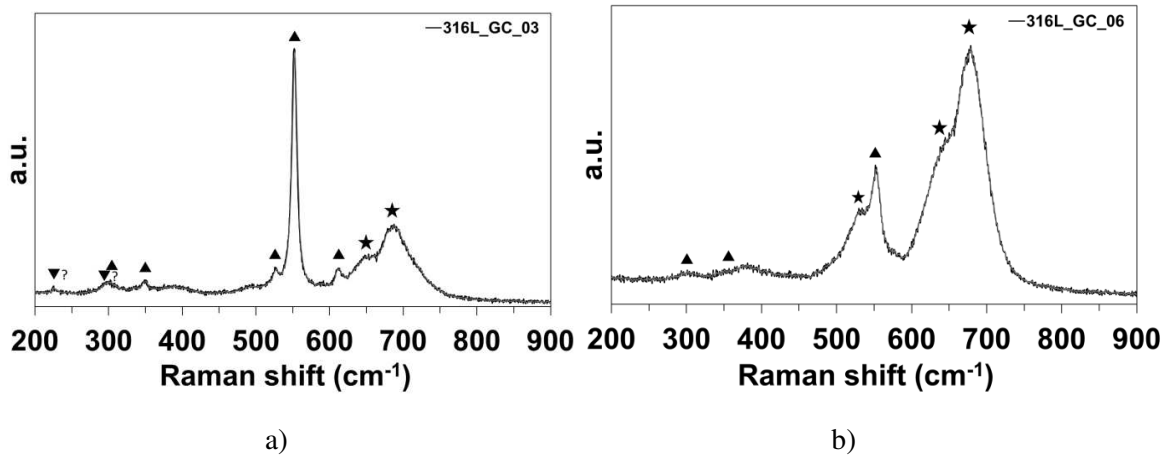


**Figure 14.** Raman spectra for the 316Ls sample oxidized in situ at 2000 Pa, after emissivity measurement at different locations on the surface ( $\blacktriangle$   $\text{Cr}_2\text{O}_3$ ;  $\star$  Spinel;  $\blacktriangledown$   $\text{Fe}_2\text{O}_3$ )

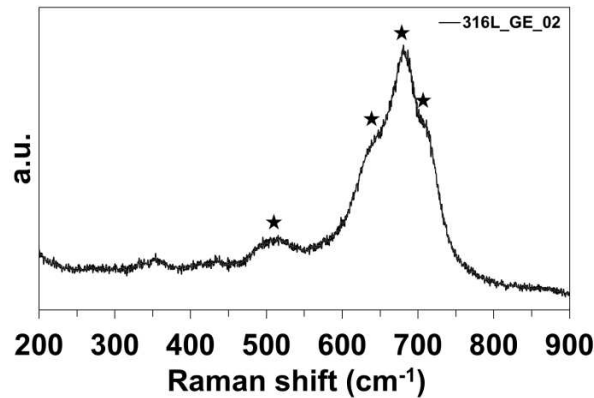


**Figure 15.** Raman spectra for the 316Ls sample oxidized in situ at atmospheric pressure, after emissivity measurement ( $\star$  Spinel)

In conclusion, the quite different compositions of the oxide layers formed during in situ oxidation at the three pressures are less influent compared to the role of the surface roughness. The total hemispherical emissivity measured is the same for the three total air pressures for the same roughness of the samples as shown in Figure 10.

## 5. Conclusions


The emissivity of 316L stainless steel samples: as-received (virgin), pre-oxidized in air plasma and oxidized in situ in air was measured from 1000 K up to 1650 K in different atmospheres: high vacuum, for two low total air pressures of 300 Pa and 2000 Pa concerning

the aerospace domain and at atmospheric pressure. New experimental results obtained for this material at high temperatures and different pressure conditions together with microstructural characterization using SEM, XRD, Raman spectroscopy and 3D profilometry were obtained as no data was found in the literature at such high temperatures. As expected, the emissivity of the oxidized 316L samples is much higher than the one measured in high vacuum due to the presence of the oxide layer and there are also some differences between air plasma and standard air conditions – in reduced atmospheres of 300 and 2000 Pa – with respective emissivity increase by a factor 3 and 2.5 in comparison with the virgin material. For the measurements carried out at atmospheric pressure, the increase of the emissivity is also 3 times higher compared to the virgin alloy. It was also shown that the most important parameter increasing the emissivity is the presence of the oxide layer that also increases the surface roughness whatever the chemical composition (hematite, magnetite, chromia and spinels) that can be a little bit different according to the total pressure as shown by the XRD and Raman analyses.

## 6. Acknowledgments

The authors thank L. Charpentier and C. Pellegrini for the surface roughness measurements. This work was partly supported by the Centre National d'Etudes Spatiales CNES, France under contract number CNES 170050 and by the Programme "Investissements d'Avenir" (Investment for the Future) of the Agence Nationale de la Recherche (National Agency for Research) of the French State under award number ANR-10-EQPX-49-SOCRATE.

## 7. References

- [1] Omaly P., Spel M., DEBRISK, a tool for re-entry risk analysis, Proc. 5<sup>th</sup> IAASS Conf. 'A Safer Space for a Safer World', Versailles (Fr), 2011, ESA SP-699. 
- [2] Omaly P., Annaloro J., DEBRISK V3: CNES tool evolutions for re-entry risk analysis, Proc. 10<sup>th</sup> IAASS Conf. 'Making Safety Happens', Los Angeles (USA), 2019.
- [3] Isetti C., Nannei E., Influence of surface treatment on the total normal emittance of AISI 316 stainless steel, *Wärme-und Stoffübertragung* 14, 1980, 211-215.
- [4] Jones P. D., Nisipeanu E., Spectral-directional emittance of thermally oxidized 316 stainless steel, *Int. J. Thermophys.* 17 (4), 1996, 967-978.
- [5] Cao G., Weber S.J., Martin S.O., Sridharan K., Anderson M.H., Allen T.R., Spectral emissivity of candidate alloys for very high temperature reactors in high temperature air environment, *J. Nucl. Mater.* 441, 2013, 667-673.

- [6] Shi D., Zou F., Zhu Z., Sun J., Modeling the effect of surface oxidation on the normal spectral emissivity of steel 316L at 1.5  $\mu\text{m}$  over the temperatures ranging from 800 to 1100 K in air, *Infrared Phys. Technol.* 71, 2015, 370-377.
- [7] Hunnewell T.S., Walton K.L., Sharma S., Ghosh T.K., Tompson R.V., Viswanath D.S., Loyalka S.K., Total hemispherical emissivity of SS 316L with simulated very high temperature reactor surface conditions, *Nucl. Technol.* 198 (3), 2017, 293-305.
- [8] Al Zubaidi F.N., Walton K.L., Tompson R.V., Ghosh T.K., Loyalka S.K., The effect of long-term oxidation on the total hemispherical emissivity of type 316L stainless steel, *Nucl. Technol.* 205 (6), 2019, 790-800.
- [9] Balat-Pichelin M., Robert J.F., Sans J.L., Emissivity measurements on carbon-carbon composites at high temperature under high vacuum, *Appl. Surf. Sci.* 253, 2006, 778-783.
- [10] Brodu E., Balat-Pichelin M., Sans J.-L., Kasper J.C., Influence of roughness and composition on the total emissivity of tungsten, rhenium and tungsten-25% rhenium alloy at high temperature, *J. Alloys Compds.* 585, 2014, 510-517.
- [11] Hernandez D., Sans J.L., Netchaieff A., Ridoux P., Le Sant V., Experimental validation of a pyroreflectometric method to determine the true temperature on opaque surface without hampering reflections, *Measurement* 42, 2009, 836-843.
- [12] Balat-Pichelin M., Sans J.L., Bêche E., Flaud V., Annaloro J., Oxidation and emissivity of Inconel 718 alloy as potential space debris during its atmospheric entry, *Mater. Charac.* 127, 2017, 379-390.
- [13] Barka L., Balat-Pichelin M., Sans J.L., Bêche E., Oxidation and emissivity of Invar 36 alloy in air plasma at high temperatures, *J. Alloys Compds.* 772, 2019, 1003-1016.
- [14] Balat-Pichelin M., Barka L., Behavior of TA6V alloy at high temperature in air plasma conditions - Part 1: oxidation, *J. Mater. Eng. & Perform.* 2020 (9 p.), 26/07/2020, DOI: 10.1007/s11665-020-04984-7
- [15] Balat-Pichelin M., Annaloro J., Barka L., Sans J.L., Behavior of TA6V alloy at high temperature in air plasma conditions - Part 2: thermal diffusivity and emissivity, *J. Mater. Eng. & Perform.* 2020 (11 p.), 28/07/2020, DOI: 10.1007/s11665-020-04985-6
- [16] Lenaz D., Lughì V., Raman study of  $\text{MgCr}_2\text{O}_4\text{-Fe}^{2+}\text{Cr}_2\text{O}_4$  and  $\text{MgCr}_2\text{O}_4\text{-MgFe}_2^{3+}\text{O}_4$  synthetic series: the effects of  $\text{Fe}^{2+}$  and  $\text{Fe}^{3+}$  on Raman shifts, *Phys. Chem. Miner.* 40(6), 2013, 491-498.
- [17] Kharbish S., Raman spectroscopic features of Al- $\text{Fe}^{3+}$ -poor magnesiochromite and  $\text{Fe}^{2+}$ - $\text{Fe}^{3+}$ -rich ferrian chromite solid solutions, *Miner. Petrol.*, 2017 (12p.), 29/08/2017 DOI 10.1007/s00710-017-0531-1



- [18] Lughì V., Lenaz D., Bonifacio A., Princivalle F., Sergio V., Parisi F., A Raman spectroscopy study of the oxidation processes in synthetic chromite  $\text{FeCr}_2\text{O}_4$ , *Ceram. Int.* 46, 2020, 29382-29387.
- [19] D'Ippolito V., Andreozzi G.B., Bersani D., Lottici P.P., Raman fingerprint of chromate, aluminate and ferrite spinels, *J. Raman Spectrosc.* 46, 2015, 1255-1264, DOI 10.1002/jrs.4764
- [20] Gomes A.S.O., Yaghini N., Martinelli A., Ahlberg E., A micro-Raman spectroscopic study of  $\text{Cr}(\text{OH})_3$  and  $\text{Cr}_2\text{O}_3$  nanoparticles obtained by the hydrothermal method, *J. Raman Spectrosc.*, 2017 (8 p.), DOI 10.1002/jrs.5198
- [21] Wang Z., Saxena S.K., Lazor P., O'Neill H.S.C., An in situ Raman spectroscopic study of pressure induced dissociation of spinel  $\text{NiCr}_2\text{O}_4$ , *J. Phys. Chem. Solids* 64, 2003, 425-431
- [22] Hosterman B.D., Farley J.W., Johnson A.L., Spectroscopic study of the vibrational modes of magnesium nickel chromite,  $\text{Mg}_x\text{Ni}_{1-x}\text{Cr}_2\text{O}_4$ , *J. Phys. Chem. Solids* 74, 2013, 985-990, DOI: 10.1016/j.jpcs.2013.02.017